Optoacoustic tomographic imaging of myelinated structures in rodent brains

Joshua Lockwood[1], Dene Ringuette[1], Xun Zhou[2], Yeni Yucel[2], and Ofer Levi[1,3,*]

[1]*The Institute of Biomaterials and Biomedical Engineering, University of Toronto, 164 College Street, Toronto, Ontario, M5S 3G9, Canada*

[2]*Department of Ophthalmology & Vision Sciences, Laboratory Medicine & Pathobiology, University of Toronto, Keenan Research Centre for Biomedical Science, 209 Victoria St, Toronto, ON M5B 1T8*

[3]*The Edward S. Rogers Sr. Department of Electrical and Computer Engineering, University of Toronto, 164 College Street, Toronto, Ontario, M5S 3G9, Canada*

**ofer.levi@utoronto.ca*

Abstract: Myelinated structures in rodent brains were identified using multispectral optoacoustic tomography; exploiting the 930 nm lipid absorbance maximum. Results support optoacoustic imaging as an inventigative tool for rodent models of multiple sclerosis.

OCIS codes: 110.4234 Multispectral and hyperspectral imaging, 170.5120 Photoacoustic imaging

1. Introduction

Neurological disorders as a whole represent a significant cost in quality of life and financial burden to countries. multiple sclerosis (MS) affects aproximately 2.5 million people worldwide and has an estimated annual cost of $34k per person in the United States [1]. One of the major road blocks to treating these neurological disorders effectively is the ability to image the affected areas of the brain. The emerging field of photoacoustic (PA) imaging promises to provide a cost-efficient and reliable way for anatomical and functional imaging of the brain. In PA imaging, pulsed lasers are employed to induce rapid thermal expansion due to optical absorption. The expansion produces short ultrasound (US) pulses which can be localized using US transducers (see in Fig. 1). Using multiple wavelength laser pulses enables discrimination of tissue composition [2]. Previous work with PA tomography, characterizing tumors in breasts, demonstrated the identification of varied concentrations of the major tissue chromophores: deoxyhemoglobin (HbR), oxyhemoglobin (HbO_2), water, and lipid. However, limited work has been done with respect to spectral unmixing of PA signal in brain imaging [3]. Myelinated axonal tracts contain a higher percentage of lipid, which has a spectroscopic absorption maximum just below the near-infrared (NIR) window [4]. In this work, we identified myelinated deep brain structures with multispectral optoacoustic tomography (MSOT). We seek to optimize MSOT analysis for the investigation demyelination in rodent disease models of MS.

2. Methods

We used an MSOT imaging system (iThera Medical Inc., Munich, Germany) with tunable 680-980 nm oscillator laser (Phocus | Opotek Incorporated, Carlsbad, California). The system partitions 630 optic fibers into 10 arms to allow for cylindrical focusing and a full 360° view of the sample. The effective spatial resolution of the array is 150 μm in plane and 800 μm elevational [5]. Three distinct experiments were carried out to examine the viability of mapping lipid content of brain using MSOT imaging: lipid phantom, ex-vivo rat brain and in-vivo mouse brain. In all experiments, imaging was performed using wavelengths between 680 nm and 980 nm at 1 nm intervals. To examine spectral discrimination of lipid, experiments were conducted using two cylindrical phantoms with 18% and 27% lipid content. The phantoms were secured within a water filled plastic bag during imaging chamber. Ex-vivo imaging was conducted on a rat brain, which was extracted after a cardiac perfusion using phosphate buffer saline. The brain was suspended inside plastic foil during imaging. In-vivo imaging was performed on a CD-1 mouse (P.28). The mouse was anesthetized using 5% isoflurane. Hair was removed from the head and neck of the mouse using an electric shaver and depilatory cream. The mouse was secured within a plastic foil hammock that prevented water from contacting the mouse. Degased ultrasound gel was applied between the plastic foil and the specimen in both the *ex vivo* and *in vivo* procedures.

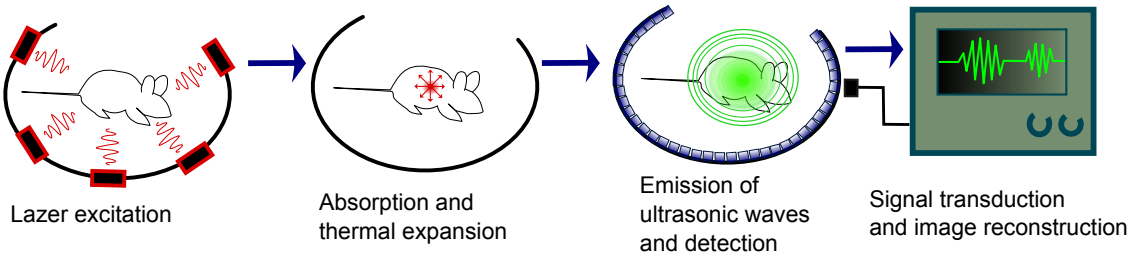

Fig. 1. Physical principle of operation for multispectral optoacoustic tomography imaging system.

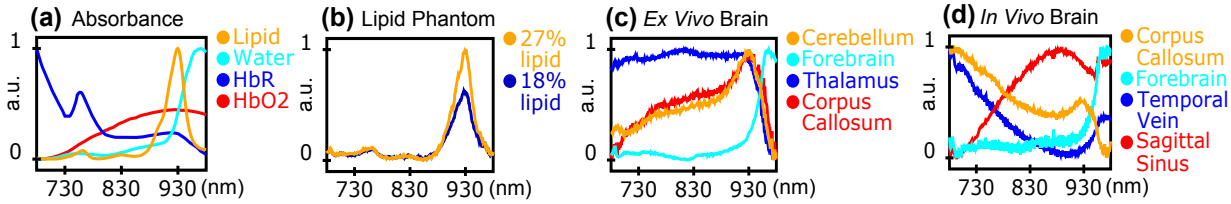

Fig. 2. Multispectral absorbance due to endogenous tissue chromophores. **(a)** Normalized molecular extinction coefficients. Spectal dependence of reconstructed PA signal for **(b)** lipid phantom, **(c)** *ex vivo* rat brain and **(d)** *in vivo* mouse brain. The regions of interest for (c) and (d) are shown in Fig. 3.

3. Results and Discussion

The tomographic reconstruction of the lipid phantoms produced regions with spectral profiles that were highly correlated, $R = 0.99 \pm 0.001$, with the NIR absorption spectrum for lipids $\varepsilon_{\text{lipid}}(\lambda)$ (see Fig. 2(b) *vs.* (a)). These regions were located close to the periphery of the phantom. Between the most highly correlated regions of each phantom, the ratio of the spectral peaks around the 930 nm lipid peak was 62% (after normalization to $\varepsilon_{\text{lipid}}(\lambda)$ for ratio preservation). This measured ratio is comparable to the 50% difference in lipid content between the phantoms. The spectral signal peak at 765 nm was also represented in both phantom measurements but the ratios were not comparable to content differences. Regions near the center of the phantoms where poorly correlated with the $\varepsilon_{\text{lipid}}(\lambda)$. However, the difference between the spectra of the central regions were still highly correlated, $R = 0.92 \pm 0.01$, with the $\varepsilon_{\text{lipid}}(\lambda)$. Consequently, differences in content can potentially be enhanced through appropriate referencing.

Ex-vivo imaging of a rat brain produced noisier spectral measurements, likely due to contributions from other chromophores (see Fig 2(c)). The main chromophores within brain tissues are: HbO_2, HbR, water, and lipid (see Fig. 2(a)). The absorption coefficient $\mu_a(\lambda)$ was modeled as a linear combination of molar extinction coefficients $\varepsilon_x(\lambda)$ and unknown concentrations $[x]$. The concentrations were inferred from a multivariate linear regression of an overdetermined system. A constant terms was included to offset negative values associated with the backprojection algorithm; improving the resolution of our composition maps. Shown from a sagittal perspective across the mid-line (see Fig. 3(a)-*i*-*iii*), regions measuring high in lipid corresponded to highly myelinated brain structures, such as the cerebellum and corpus callosum. The fine tree-like structure of myelin in the cerebellum [6] is distinct in Fig. 3(a)-*ii*. Conversely, regions measuring high in water corresponded to un-myelinated grey matter regions such as the forebrain. Furthermore, the $\mu_a(\lambda)$ of both the cerebellum and corpus callosum were highly correlated, $R = 0.83 \pm 0.02$ and $R = 0.72 \pm 0.03$, with the $\varepsilon_{\text{lipid}}(\lambda)$ and conversely, the forebrain was highly correlated with $\varepsilon_{\text{water}}(\lambda)$ $R = 0.97 \pm 0.003$. The HbR and HbO_2 spectrum is due to residual blood (in Fig. 3(a)-*iii*). The accumulation of HbR in grey matter may to due to its greater metabolic demand being maintained shortly after perfusion. Coronal perspectives the cerebellum and the pericentral regions reiterate the spatial distribution (see Fig. 3(a)-*iv*-*vi* & *vii*-*ix*, respectively).

For the *in vivo* mouse brain imaging experiment, the same analysis was performed. Due to significant artifacts from the skull the signal quality was lower (see Fig 3(b)-*i*), but the ability to detect the lipid content of central brain structures was maintained (see Fig 3(b)-*ii*). The peak in the $\varepsilon_{\text{lipid}}(\lambda)$ at 930 nm was evident but a large quasi-linear rise in absorbance with decreasing wavelength (see Fig. 2(d)). Subtracting the linear trend (computed through linear regression) resulted in a spectral profile highly correlated $R = 0.71 \pm 0.03$ with the lipid spectrum. Other regions (see

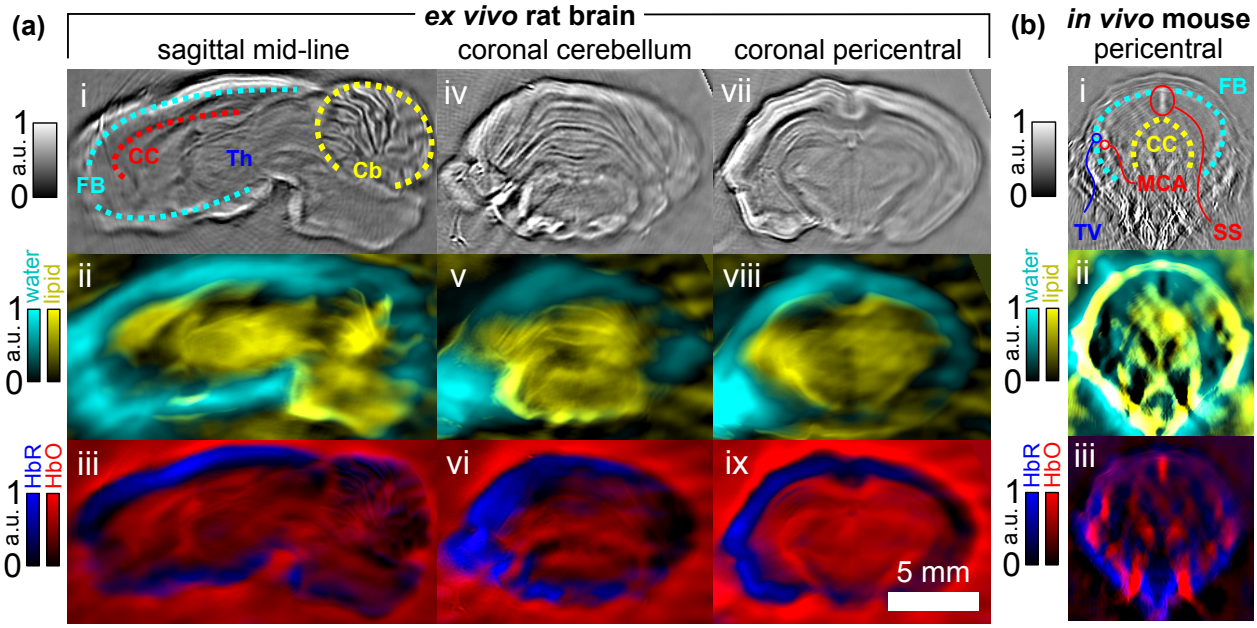

Fig. 3. Imaging of tissue composition with MSOT. **(a)** An *ex vivo* rat brain and **(b)** An *in vivo* mouse brain. (**i**, iv, vii) High-pass filtered 680 nm images, (**ii**, v, viii) Lipid *(yellow)* and water *(cyan)* composition maps, and (**iii**, vi, ix) are HbR *(blue)* and HbO_2 *(red)* composition maps.

Fig 3 (b)-*iii*) were highly correlated with the other chromophores without linear correction: HbO_2 in the sagittal sinus ($R = 0.969 \pm 0.003$) and middle cerebral artery ($R = 0.72 \pm 0.03$), HbR in the temporal vein ($R = 0.84 \pm 0.02$), and, water in forebrain regions without a large vessel $R = 0.95 \pm 0.01$. Consequency, it is not know what contribution of the linear spectral trend in the corpus callosum is due to the presence of other chromophores or interference from the skull. Regardless, artifacts in the computed lipid profile appear to be largely limited to a first order bias.

4. Significance and conclusions

We have shown that MSOT imaging is able to locate differences in lipid content between rodent brain structures. For regions of interest where the 930 nm lipid absorbance peak is distorted referencing or linear correction restore the spectral correlation. This demonstrates the potential for studying demyelination in disease models such as multiple sclerosis. Ultimately MSOT could become a cost-efficient and portable method for clinical diagnosis.

References

1. K. Whetten-Goldstein, F. A. Sloan, L. B. Goldstein, and E. D. Kulas, "A comprehensive assessment of the cost of multiple sclerosis in the United States," Multiple sclerosis **4**, 419–425 (1998).
2. S. Zackrisson, S. van de Ven, and S. Gambhir, "Light in and sound out: emerging translational strategies for photoacoustic imaging," Cancer Research **74**, 979–1004 (2014).
3. B. J. Tromberg, Z. Zhang, A. Leproux, T. D. O'Sullivan, A. E. Cerussi, P. M. Carpenter, R. S. Mehta, D. Roblyer, W. Yang, K. D. Paulsen *et al.*, "Predicting responses to neoadjuvant chemotherapy in breast cancer: Acrin 6691 trial of diffuse optical spectroscopic imaging," Cancer Research **76**, 5933–5944 (2016).
4. A. Cerussi, N. Shah, D. Hsiang, A. Durkin, J. Butler, and B. J. Tromberg, "In vivo absorption, scattering, and physiologic properties of 58 malignant breast tumors determined by broadband diffuse optical spectroscopy," Journal of Biomedical Optics **11**, 044,005–044,005 (2006).
5. A. Buehler, E. Herzog, D. Razansky, and V. Ntziachristos, "Video rate optoacoustic tomography of mouse kidney perfusion," Optics Letters **35**, 2475–2477 (2010).
6. D. R. Foran and A. C. Peterson, "Myelin acquisition in the central nervous system of the mouse revealed by an mbp-lac z transgene," The Journal of Neuroscience **12**, 4890–4897 (1992).